Journal of Power Sources 267 (2014) 821–830

Contents lists available at ScienceDirect

Journal of Power Sources

journal homepage: www.elsevier.com/locate/jpowsour

Combined quantum chemical/Raman spectroscopic analyses of Li^+ cation solvation: Cyclic carbonate solvents—Ethylene carbonate and propylene carbonate

Joshua L. Allen [a, b], Oleg Borodin [b], Daniel M. Seo [a], Wesley A. Henderson [a, c, *]

[a] Ionic Liquids & Electrolytes for Energy Technologies (ILEET) Laboratory, Department of Chemical & Biomolecular Engineering, North Carolina State University, Raleigh, North Carolina 27695, USA
[b] Electrochemistry Branch, U.S. Army Research Laboratory, Adelphi, Maryland 20783, USA
[c] Electrochemical Materials & Systems Group, Energy & Environment Directorate, Pacific Northwest National Laboratory (PNNL), Richland, Washington 99352, USA

HIGHLIGHTS

- DFT calculations used to examine EC and PC coordination to lithium cations.
- A methodology is provided to accurately determine EC solvation numbers.
- PC solvation numbers cannot be accurately determined from a Raman analysis.

GRAPHICAL ABSTRACT

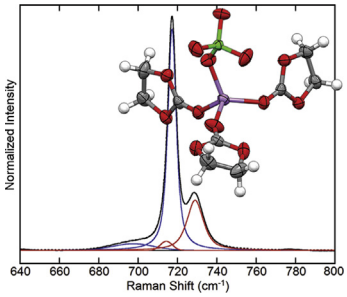

ARTICLE INFO

Article history:
Received 30 January 2014
Received in revised form
16 April 2014
Accepted 20 May 2014
Available online 2 June 2014

Keywords:
Battery
Electrolyte
Solvation number
Ethylene carbonate
Propylene carbonate
Raman spectroscopy

ABSTRACT

Combined computational/Raman spectroscopic analyses of ethylene carbonate (EC) and propylene carbonate (PC) solvation interactions with lithium salts are reported. It is proposed that previously reported Raman analyses of $(EC)_n$–LiX mixtures have utilized faulty assumptions. In the present studies, density functional theory (DFT) calculations have provided corrections in terms of both the scaling factors for the solvent's Raman band intensity variations and information about band overlap. By accounting for these factors, the solvation numbers obtained from two different EC solvent bands are in excellent agreement with one another. The same analysis for PC, however, was found to be quite challenging. Commercially available PC is a racemic mixture of (*S*)- and (*R*)-PC isomers. Based upon the quantum chemistry calculations, each of these solvent isomers may exist as multiple conformers due to a low energy barrier for ring inversion, making deconvolution of the Raman bands daunting and inherently prone to significant error. Thus, Raman spectroscopy is able to accurately determine the extent of the EC…Li^+ cation solvation interactions using the provided methodology, but a similar analysis of PC…Li^+ cation solvation results in a significant underestimation of the actual solvation numbers.

* Corresponding author. Electrochemical Materials & Systems Group, Energy & Environment Directorate, Pacific Northwest National Laboratory (PNNL), Richland, Washington 99352, USA. Tel./fax: +1 509 375 2426.
E-mail addresses: oleg.a.borodin.civ@mail.mil (O. Borodin), Wesley.Henderson@pnnl.gov (W.A. Henderson).

http://dx.doi.org/10.1016/j.jpowsour.2014.05.107
0378-7753/

1. Introduction

Electrolytes have become the limiting component for next-generation lithium batteries with regard to implementing advanced electrodes, improving safety, operation at high and/or low-temperature, etc. Electrolyte properties are directly related to the cation solvation interactions present in solution. In particular, in order to achieve a high battery rate performance (power), the ionic conductivity of electrolyte solutions is of upmost importance. As this is a direct reflection of the transport properties of the ions, it is highly dependent upon the ionic association tendency of the anions (i.e., anion…Li^+ cation interactions). One reason that $LiPF_6$ is predominantly used as the electrolyte salt for commercial Li-ion batteries is that this salt dissociates extensively into fully solvated Li^+ cations and uncoordinated PF_6^- anions resulting in exceptionally high ionic conductivity values. The anion…Li^+ cation interactions are minimized by the weakly coordinating PF_6^- anions, thus reducing or eliminating the formation of contact ion pair (CIP) and aggregate (AGG) solvates. The extent of the ionic association interactions present within an electrolyte, however, are dictated not only by ionic association tendency of the anions, but also by the strength of the ionic solvation (solvent…Li^+ cation) interactions; thus the anions and solvent molecules directly compete with one another for coordination to the Li^+ cations within the coordination shells of the cations (which typically consist of four or five coordinated donor atoms from the anions and/or solvent molecules, except for multidentate coordinating solvents such as glymes for which the coordination number can be as high as eight [1]). Scrutinizing the solvation interactions present within electrolyte mixtures is therefore imperative to obtain a comprehensive understanding of the origin of electrolyte properties and for facilitating the tuning of these properties for particular battery applications/requirements.

Recent work by the authors has focused on determining the solution structure of acetonitrile–lithium salt mixtures (i.e., $(AN)_n$–LiX electrolytes) and then linking this directly to the electrolyte properties [2–5]. The present study was found to be necessary to extend this characterization to electrolytes with the cyclic carbonate solvents ethylene carbonate and propylene carbonate (i.e., $(EC)_n$–LiX and $(PC)_n$–LiX mixtures). Numerous experimental Raman spectroscopic studies have been previously reported on the Li^+ cation solvation in such electrolytes [6–17]. The present study, however, suggests that these studies have inherent flaws in the analysis methodologies utilized which is evident from the inconsistent and sometimes confusing results about solvation interactions obtained from them.

Joint computational/experimental analyses were therefore conducted to rigorously scrutinize the procedures for obtaining solvation numbers for electrolyte mixtures with EC or PC and lithium salts. DFT calculations were used to determine the actual (rather than apparent) Raman vibrational bands present and their corresponding Raman activity (to calculate the scaling factors). This information was then directly applied for the analysis of the solvation numbers from the experimental data. More explicitly, the accurate evaluation of this experimental data is dependent upon the consideration of both Raman band overlap and scaling—two critical factors (obtained from the computational evaluation) which have been neglected in previous publications. These previous analyses relied heavily on (invalid) assumptions. Using the reported methodology, however, consistent solvation numbers are obtained when analyzing two different EC solvent bands. In addition, a detailed explanation is provided for why the determination of PC solvation numbers using Raman spectroscopy is inherently flawed and thus results in the calculation of highly erroneous solvation numbers.

2. Experimental

2.1. Materials and sample preparation

The solvents EC and PC (Novolyte, electrolyte grade) were used as-received. Isomerically pure (*S*)-PC and (*R*)-PC were purchased from Sigma–Aldrich and used as-received. The salts $LiPF_6$ (Novolyte, electrolyte grade), $LiBF_4$ (Novolyte, electrolyte grade), $LiClO_4$ (Novolyte, electrolyte grade) and $LiCF_3SO_3$ (Sigma–Aldrich, 99.995%) were used as-received, while LiTFSI (3 M) and $LiCF_3CO_2$ (Sigma–Aldrich, 95%) were dried under high vacuum at 120 °C for 24 h prior to use. Samples were prepared in a Vacuum Atmospheres inert atmosphere (N_2) glovebox (<1 ppm H_2O) by adding the appropriate amount of each solvent to the lithium salts in hermetically-sealed vials and heating/stirring until homogenous solutions were obtained. The water content of the electrolytes was verified to be less than 20 ppm using a Mettler Toledo DL39 Karl Fischer coulometer.

2.2. Thermal analysis

DSC measurements were performed with a TA Instruments Q2000 DSC with liquid N_2 cooling. The instrument was calibrated with cyclohexane (solid–solid phase transition at −87.06 °C, melt transition (T_m) at 6.54 °C) and indium (T_m at 156.60 °C). Hermetically-sealed Al sample pans were prepared in the glovebox. Sample pans were cycled (5 °C min^{-1}) and annealed repeatedly at subambient temperature to fully crystallize the samples. Once the samples were crystallized, the pans were cooled to −150 °C and then heated (5 °C min^{-1}) to fully melt the samples. Only the final heating traces are reported. Peak temperatures from this data were then used to construct the (*S*)- and (*R*)-PC phase diagram.

2.3. Raman spectroscopic measurements

Raman spectroscopic measurements were performed on a Horiba-JobinYvon LabRAM HR VIS high resolution confocal microscope using a 632 nm^{-1} He–Ne laser as the excitation source and a Linkam stage for temperature control and protection from ambient moisture. A 50X long distance optical objective was used with the Linkam stage. The instrument was calibrated with a monocrystalline Si wafer at 520.7 cm^{-1}. Spectra were typically collected using a 20–30 s exposure time and 20 accumulations to ensure high resolution spectra were obtained. Raman spectra were deconvoluted with a Gaussian–Lorentzian function using LabSpec software.

2.4. DFT calculations

Most of the DFT calculations were performed using a B3LYP functional that showed excellent predictive capabilities for the Raman spectra of the solvents [18]. A limited set of calculations was also performed using M06-L and M05-2X density functionals. The M06-L (local) functional was chosen because it yielded the most accurate EC/Li^+ binding energy among the functionals tested (LC-wPBE, M05-2X, B3LYP and HSE06). Both small 6-31 + G(d,p) and large aug-cc-pvTz (denoted as Tz) basis sets were used. A polarized continuum model (PCM) with either EC or PC parameters was employed in all of the calculations to implicitly incorporate solvation effects, unless noted otherwise. For clarity, Raman bands calculated by DFT analysis are preceded by "*ca*", whereas Raman bands that do not contain *ca* are indicative of experimental results. Solvent molecules coordinated to Li^+ cations have been denoted as $solvent_n/Li^+$ or $solvent_n$/LiX when

referring to the quantum chemical calculations and (solvent)$_n$–LiX when referring to experimental mixtures. Calculated Raman spectra were obtained using the SWizard program with a Gaussian band shape and a full-width-at-half-maximum (FWHM) of 15 cm^{-1} [19,20].

3. Results and discussion

3.1. (EC)$_n$–LiX Raman analysis

The experimental Raman spectra of EC at 60 °C (liquid) and −80 °C (crystalline solid) are shown in Fig. 1. Numerous vibrational spectroscopic investigations have been reported for (EC)$_n$–LiX mixtures in which two Raman EC solvent bands, in particular, have been reported to shift upon solvent coordination to a Li^+ cation—i.e., ring bending and ring breathing modes [6,9,10,12,21–23]. Some controversy exists, however, as to the correct assignment of these bands. Durig et al. attributed the band at 717 cm^{-1} to a skeletal bending mode with A_1 symmetry after concluding that this bending mode could not be due to a C=O ring bending vibration because of its polarized nature [22]. This is consistent with a study performed by Dorris et al. on vinylene carbonate [23]. Fortunato et al. also reported a ring bending mode at 717 cm^{-1} and a ring breathing mode at 894 cm^{-1} [21]. Conversely, Hyodo et al. and Klassen et al. have more recently associated the 714 cm^{-1} Raman band to an out-of-plane C=O ring bending vibration, whereas the 891 cm^{-1} band shares a similar assignment with the previous reports [6,12].

DFT calculations in the present work examined the vibrational modes of EC, EC$_n$/Li^+ and EC$_n$/LiX complexes with high Raman activity in the 700–900 cm^{-1} region and the C=O vibrational mode near 1800 cm^{-1}. Fig. 2 shows the Raman spectrum of an EC molecule calculated at the B3LYP/Tz and B3LYP/6-31 + G(d,p) levels with PCM(EC). The calculated vibrational modes may be directly visualized through animation of the EC molecule (see Supplemental data). The spectra indicate that the *ca* 713 and 902 cm^{-1} bands each have contributions from two vibrational modes. These vibrational modes are shown in Fig. 3. The band at *ca* 713 cm^{-1} is dominated by a vibration consisting of ring breathing with an O–C–O symmetric stretch and a minor contribution from the ring distortion with a–CH_2– rocking mode that is red shifted to *ca* 704 cm^{-1}. The ring breathing mode at *ca* 902 cm^{-1} also contains a minor left shoulder due to the–CH_2– twisting motion (*ca* 885 cm^{-1}), as shown in Fig. 2. A comparison of the spectra from the B3LYP/Tz and B3LYP/6-31 + G(d,p) calculations indicates that usage of the smaller 6-31 + G(d,p) basis set, as compared to Tz, results in no appreciable difference in the spectra. Therefore, the 6-31 + G(d,p) basis set was used for a majority of the calculations.

Although the carbonyl oxygen atoms are widely accepted to dominate the coordinate of EC to Li^+ cations, the complexity of the overlapping carbonyl Raman bands makes their experimental deconvolution impractical. The C=O stretching vibration, calculated to be a single band at *ca* 1808 cm^{-1}, is natively split into two bands (Fig. 1). These bands exist primarily as a consequence of Fermi resonance of the C=O stretching mode with an overtone of the ring breathing mode [24,25]. Once coordinated to a Li^+ cation, these bands are each shifted, further increasing the complexity of

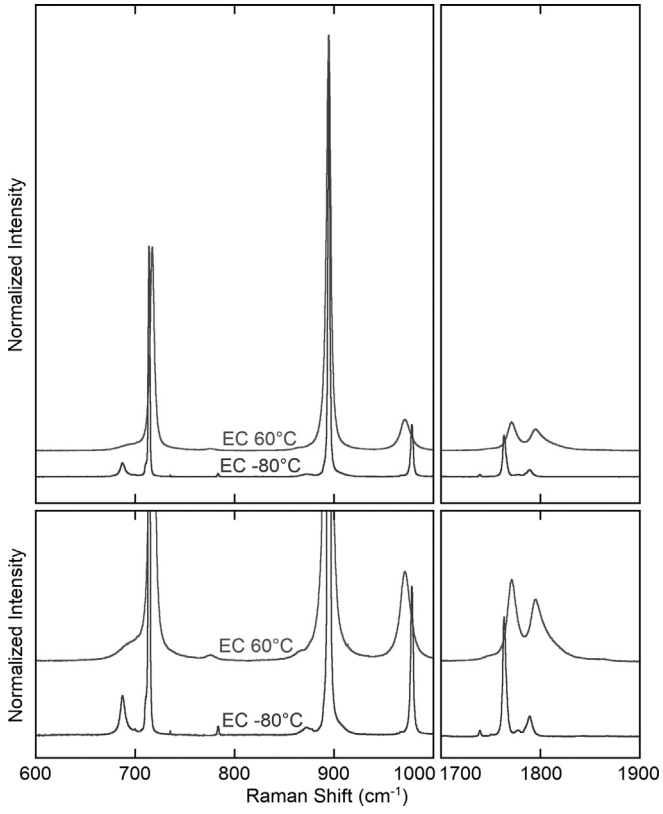

Fig. 1. Comparison of the experimental Raman spectra of EC at 60 °C (liquid) and −80 °C (crystalline solid).

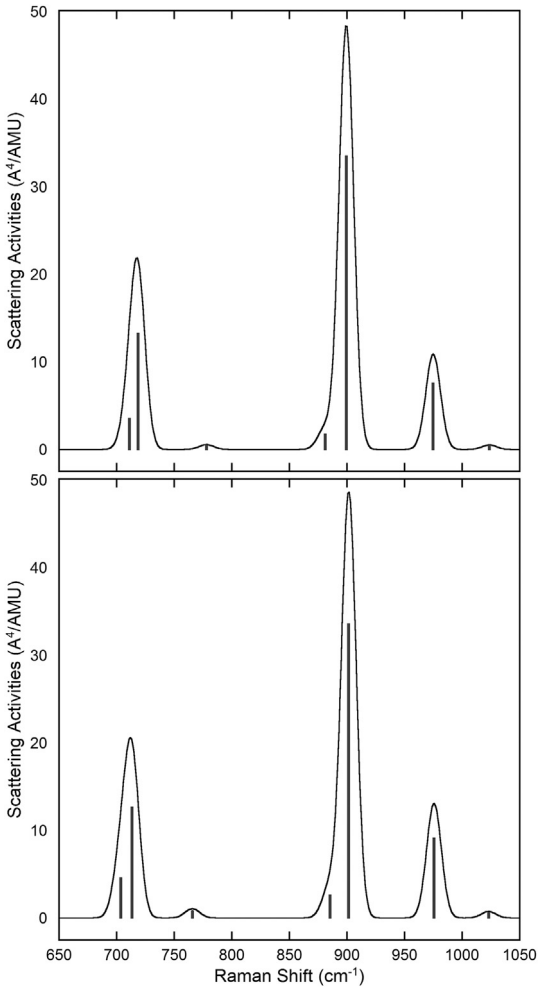

Fig. 2. Raman spectra for EC from (top) B3LYP/Tz and (bottom) B3LYP/6-31 + G(d,p) calculations with PCM(EC).

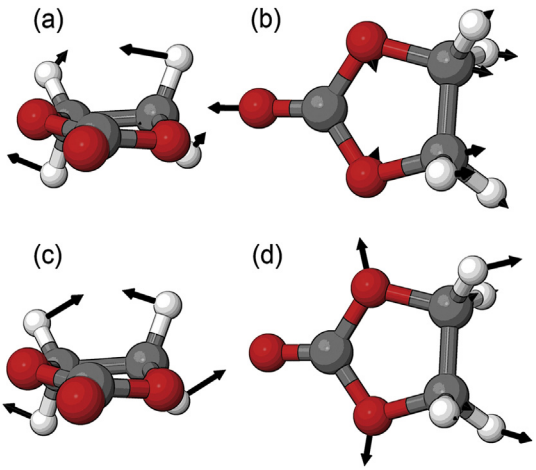

Fig. 3. Vibrational modes of EC from the B3LYP/6-31 + G(d,p) calculations with PCM(EC) for (a) ring distortion with–CH_2– rocking at *ca* 704 cm^{-1}, (b) ring breathing with O–C–O symmetric stretch at *ca* 713 cm^{-1}, (c) –CH_2– twisting symmetric with respect to C_{2V} symmetry plane at *ca* 885 cm^{-1} and (d) ring breathing symmetric with respect to C_{2V} at *ca* 902 cm^{-1} (see Supplemental data for animation).

the analysis. Due to the difficulties of deconvoluting these bands, and the compounding errors associated with such an analysis, the evaluation of the carbonyl stretching bands has not been performed in the present study.

Most quantum chemical studies to date have focused on examining the Raman spectra of gas-phase solvent and solvent/Li^+ clusters, while largely neglecting condensed phase effects [26–28]. The influence of including the implicit (PCM) and explicit interactions between solvent molecules, the latter by comparing a cluster of EC molecules (i.e., EC_4) to a single molecule (i.e., EC_1), on the Raman spectra was examined in the present study with the results reported in Table 1. Inclusion of PCM for the EC_1 calculations results in a significant frequency shift of up to 11 cm^{-1} for bands below 940 cm^{-1} and 80–100 cm^{-1} for the C=O vibration. The PCM inclusion also increased the Raman band activities, but, importantly, the increase was not uniform for all of the bands—i.e., the increase ranged from a factor of 1.6–2.2. A comparison of the EC_4 vs. EC_1 Raman spectra predictions indicates smaller shifts of the average band positions as compared to the initial inclusion of the PCM model for EC. Interestingly, the explicit consideration of EC_4 does change the Raman band activities by factors ranging from 0.8 to 1.4. A comparison of the predicted spectra for EC_4 and EC_1 with the experimental data for EC, shown in Fig. 1, indicates a slightly better agreement for the EC_4 spectrum (Fig. S3) with experiments, but the differences are minor. Experimental deconvolution is able to adequately model the shoulder present at *ca* 704 cm^{-1}, but the shoulder for the *ca* 885 cm^{-1} band in the experimental EC spectrum is negligible.

When an EC molecule coordinates a Li^+ cation, the vibrational bands mentioned previously are shifted. While previous DFT calculations of EC_1 and EC_1/Li^+ were performed for the isolated solvent and complex in vacuum [26,27], the present calculations were performed with PCM(EC) to implicitly account for solvent effects. When PCM is not included, the EC polarization by the Li^+ cation is dramatically overestimated for EC_1/Li^+ and much larger clusters are needed to correct for this artifact [26]. For example, gas phase calculations for the ring breathing mode (*ca* 719 cm^{-1} for neat EC_1 with the B3LYP/Tz functional) yielded shifts of 41–102 cm^{-1} for EC_2/Li^+, 33.5–47.5 cm^{-1} for EC_3/Li^+, and 22.1–26.7 cm^{-1} for EC_4/Li^+ [26]; these shifts are clearly decreasing with increasing cluster size. The present calculations for EC_1/Li^+ with PCM(EC), however, yield a shift of only 19–24 cm^{-1}, which is more representative of the experimental shifts observed in $(EC)_n$–LiX mixtures. Various functionals were surveyed to determine the most suitable analysis technique for comparison with the experimental data. The calculated frequency shifts and activities of the EC_1/Li^+ complex, and their relationship with EC_1, using multiple functionals is reported in the Supplemental data. Upon Li^+ cation coordination, the present calculations indicated that the EC ring breathing modes at *ca* 713 and 902 cm^{-1} are blue shifted 14–24 and 9–10 cm^{-1}, respectively (Table 2) (vs. the EC_1 data shown in Table 1 for the B3LYP/6-31 + G(d,p) with PCM(EC) calculation). The ring distortion mode (shoulder) at *ca* 704 cm^{-1}, however, is blue shifted 8–10 cm^{-1} and the *ca* 885 cm^{-1} band is slightly red shifted or does not shift upon Li^+ cation coordination (−3 to 1 cm^{-1}). Other levels of theory were found to provide quantitative agreement with these shifts (Supplemental data).

The extent to which the vibrational bands shift upon cation coordination was found to be slightly dependent upon the number of EC molecules and/or the presence of an anion in the coordination shell that surrounds the Li^+ cation, as shown in Fig. 4 (only the average activity weighted frequencies are shown for clarity). The calculated EC frequency shifts upon Li^+ cation coordination indicate a weak dependence on the number of EC molecules coordinating a Li^+ cation for the 704, 713, 885 and 902 cm^{-1} bands. In contrast to these results, previously reported gas-phase calculations (without a PCM model) indicated a dramatic dependence of the EC shifts upon Li^+ cation coordination with varying number of EC molecules in the EC_n/Li^+ cluster for $n = 1$–4 [26]. The presence of an anion as a solvent-separated ion pair (SSIP) or contact ion pair (CIP) (i.e., $EC_4/LiBF_4$ or $EC_3/LiBF_4$, respectively, in Fig. 4) had a relatively minor influence on the frequency shifts and activity ratios for the EC_n/Li^+ complexes (vs. the EC_1 solvent vibrational bands). This is an important conclusion as it supports the assumption that the frequency shifts and activity differences will be negligible upon increasing salt concentration. Thus, the frequency shifts and activity values are assumed to be independent of the salt concentration, the state of ion aggregation (i.e., SSIP vs. CIP) and the nature of the anion used in the analysis (i.e., PF_6^- vs. BF_4^-). Table 2 was

Table 1
EC Raman band frequencies (cm^{-1}) and activities (*S*).

			Frequency					Raman activity				
			$freq_1$	$freq_2$	$freq_3$	$freq_4$	$freq_5$	$freq_1$	$freq_2$	$freq_3$	$freq_4$	$freq_5$
EC_1	B3LYP	no PCM, $\varepsilon = 1$	693	715	890	892	1898	2.6	6.0	1.6	15.0	18.2
EC_1	B3LYP	PCM(EC)	704	713	885	902	1808	4.5	12.6	2.5	33.5	31.7
EC_1	M05-2X	no PCM, $\varepsilon = 1$	691	730	908	929	1961	2.1	4.8	1.6	14.5	15.7
EC_1	M05-2X	PCM(EC)	701	729	904	938	1862	3.6	9.6	2.5	31.4	26.2
EC_1	M06L	no PCM, $\varepsilon = 1$	692	721	893	901	1930	2.6	6.0	1.9	14.1	15.8
EC_1	M06L	PCM(EC)	703	721	889	910	1851	4.7	12.2	3.2	31.4	25.4
EC_4	B3LYP	PCM(EC)	711	715	884	902	1804	4.3	16.0	2.2	36.7	36.1
EC_4	M05-2X	PCM(EC)	697	732	903	939	1849	3.0	11.5	2.2	32.7	25.3

Calculations using the 6-31 + G(d,p) basis set. Activity weighted averages are given for EC_4.

Table 2
EC_3/Li^+ Raman band frequencies (cm^{-1}) and activities (S).

	$freq_1$	$freq_2$	$freq_3$	$freq_4$	$freq_5$
EC_1/Li^+ freq	712	738	882	911	1790
EC_1/Li^+ freq shift (vs. EC_1)	8	24	−3	9	−18
EC_3/Li^+ freq (avg)	713	730	885	911	1788
EC_3/Li^+ shift (EC-1)	8	14	−2	9	−26
EC_3/Li^+ shift (EC-2)	9	19	0	10	−25
EC_3/Li^+ shift (EC-3)	10	21	1	10	−17
EC_3/Li^+ shift (avg) (vs. EC_1)	9	17	0	9	−20
$S(EC_3/Li^+)$	4.95	11.08	2.44	35.40	23.63
$S(EC_3/Li^+)/S(EC_1)$	1.09	0.88	0.96	1.06	0.75

Calculations using B3LYP/6-31 + G(d,p) with PCM(EC) (average weighted by Raman activities). Bold values were used for the corrected solvation numbers in Table 3 (see Supplemental data). The uncoordinated EC_1 values refer to the B3LYP–PCM(EC) values reported in Table 1. Values rounded to the nearest integer are reported for the frequencies.

therefore generated from B3LYP/6-31 + G(d,p) with PCM(EC) calculations for the EC_1/Li^+ and EC_3/Li^+ complexes (see also the Supplemental data). Using experimental data in conjunction with the calculated Raman shifts of the EC_3/Li^+ complex, along with the fact that other 4-fold coordinated Li^+ solvates yield very similar values, it was determined that the EC_3/Li^+ complex reasonably represents the influence of Li^+ cations on the EC Raman spectrum. In order to properly interpret the experimental results, it is necessary to scale the intensities of the Raman bands to account for less/more Raman active species. Table 2 displays the calculated Raman band frequencies and relative activities for EC_3/Li^+ as compared with EC_1. The Raman activity for the *ca* 902 cm^{-1} band (shifted to *ca* 911 cm^{-1}) is largely unchanged (increased slightly) upon Li^+ cation coordination (scaling factor 1.06), while the activity of the *ca* 713 cm^{-1} band (shifted to *ca* 738 cm^{-1}) is decreased approximately 12% when compared with EC_1 (scaling factor 0.88), respectively.

The experimental Raman spectra of $(EC)_n$–LiX mixtures were deconvoluted by accounting for the calculated bands from the DFT analysis of the uncoordinated EC_1 and EC_3/Li^+ complex (using the values from the B3LYP/6-31 + G(d,p) with PCM(EC) calculations reported in Table 2). The exception to this is the Raman band at *ca* 885 cm^{-1} (frequency for both uncoordinated and Li^+ cation coordinated EC). The Raman activity of this band is quite small relative to that for the ring breathing mode (*ca* 902 cm^{-1}) (Fig. 2) and the 885 and 902 cm^{-1} bands are very difficult to experimentally deconvolute. The 885 cm^{-1} band was therefore neglected in the analysis of Li^+ cation coordination reported in Table 3. A representative Raman band deconvolution of the data from a $(EC)_n$–$LiClO_4$ ($n = 10$) mixture is shown in Fig. 5. The blue bands represent the uncoordinated EC vibrational bands (as calculated from the DFT analysis of EC_1). Upon coordination to Li^+ cations, these bands shift to a higher frequency, which is modeled as the red bands. It is noteworthy that the shoulder at 697 cm^{-1} (*ca* 704 cm^{-1}) for the uncoordinated EC is calculated to shift ~9 cm^{-1} upon coordination, which overlaps extensively with the uncoordinated ring breathing mode at 717 cm^{-1} (*ca* 713 cm^{-1}). Fitting this band, however, was fairly easily done as the 714 cm^{-1} band (i.e., shifted 697 cm^{-1} band due to Li^+ coordination) appeared as a secondary shoulder that was necessary to properly fit the spectra. The ratio of the uncoordinated and coordinated bands was used to calculate the average solvation numbers via the following formula:

$$\frac{A_C}{A_C + A_U} = N\frac{c_{LiX}}{c_S}$$

where A_C and A_U are the integrated area intensities of the vibrational bands for Li^+ cation coordinated (729 or 905 cm^{-1}) and uncoordinated (717 or 894 cm^{-1}) solvent, respectively, c_{Lix} and c_S are the concentration of the lithium salt and solvent, respectively, and N is the average solvation number.

The uncorrected solvation numbers, reported in Table 3 for $(EC)_n$–LiX mixtures, calculated using the 717/729 or 894/905 cm^{-1} solvent bands are in poor agreement with one another. The

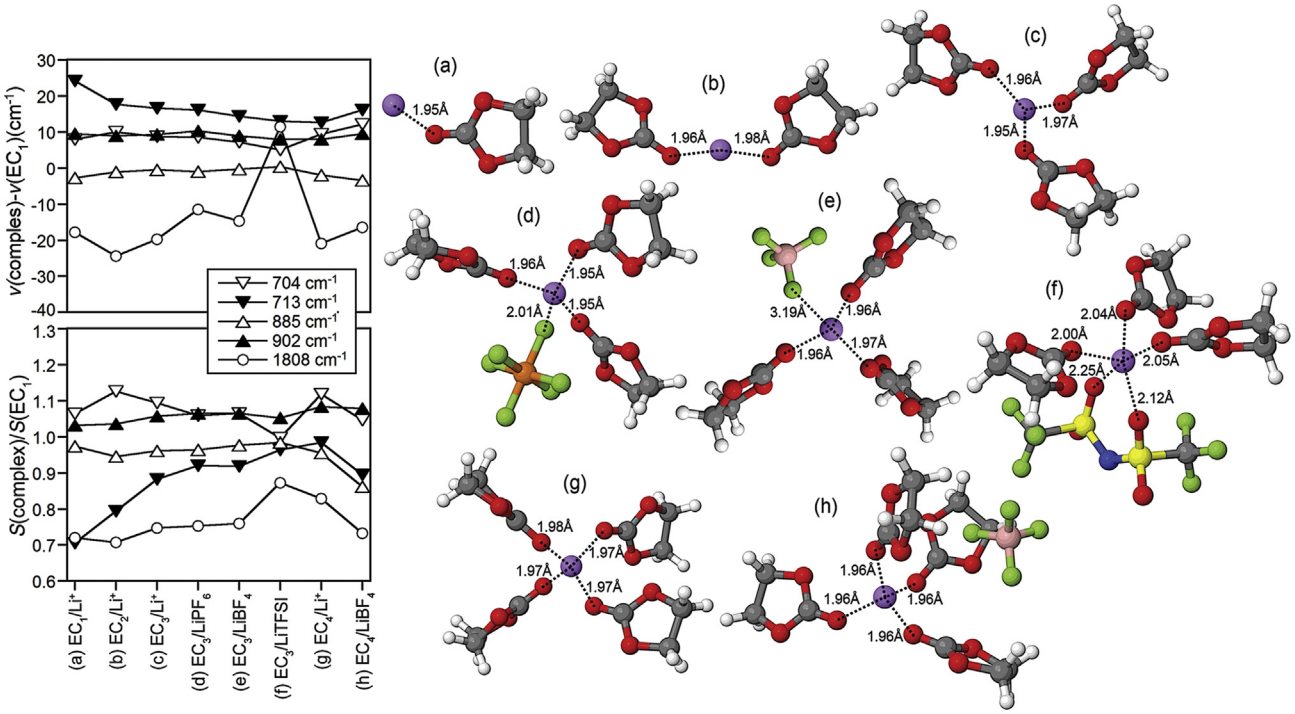

Fig. 4. Frequency shifts (cm^{-1}) and activity ratios of EC_n/Li^+ and EC_n/LiX complexes vs. EC_1 from B3LYP/6-31 + G(d,p) calculations with PCM(EC) and the corresponding coordination for (a) EC_1/Li^+, (b) EC_2/Li^+, (c) EC_3/Li^+, (d) (CIP) $EC_3/LiPF_6$, (e) (CIP) $EC_3/LiBF_4$, (f) (CIP) $EC_3/LiTFSI$, (g) EC_4/Li^+ and (h) (SSIP) $EC_4/LiBF_4$.

Table 3
Uncorrected and corrected solvation numbers (N) for $(EC)_n$–LiX mixtures ($n = 20$ and 10).

	EC/Li	729 cm^{-1}		905 cm^{-1}		Difference	
		20/1	10/1	20/1	10/1	20/1	10/1
uncorrected	$LiPF_6$	3.75	3.62	4.36	4.03	0.62	0.41
	LiTFSI	3.30	3.33	3.84	3.76	0.55	0.43
	$LiClO_4$	3.01	3.03	3.50	3.41	0.49	0.37
	$LiBF_4$	2.73	2.75	3.19	3.14	0.46	0.38
	$LiCF_3SO_3$	2.31	2.06	2.73	2.37	0.41	0.32
	$LiCF_3CO_2$	1.16	1.15	1.35	1.32	0.19	0.17
corrected	$LiPF_6$	4.15	3.92	4.17	3.89	0.02	0.03
	LiTFSI	3.66	3.62	3.66	3.62	0.00	0.00
	$LiClO_4$	3.35	3.31	3.33	3.28	0.02	0.03
	$LiBF_4$	3.05	3.01	3.04	3.01	0.01	0.00
	$LiCF_3SO_3$	2.59	2.27	2.59	2.27	0.01	0.01
	$LiCF_3CO_2$	1.30	1.28	1.28	1.25	0.03	0.03

differences in the solvation numbers obtained suggest that the analyses performed in other publications are invalid. By accounting for the overlapping second smaller Raman band at 714 cm^{-1} due to coordinated EC (Fig. 5a) (subtracting this intensity from the 717 cm^{-1} band for the uncoordinated EC) and scaling the bands by the activity ratios (scaling factors) listed in Table 2, however, the calculated ("corrected") solvation numbers converge nearly perfectly for the mixtures tested (Table 3). In addition, the anion association tendency for varying lithium salts has previously been shown to increase in the order [2–4,29]:

$$CF_3CO_2^- > CF_3SO_3^- > BF_4^- > ClO_4^- \geq TFSI^- > PF_6^-$$

The solvation numbers obtained (Table 3) are in excellent agreement with this ionic association trend (increasing solvation results in reduced ionic association as the solvent molecules and anions compete for coordination in the solvation shells of the Li^+ cations). This is evident by normalizing the intensity of the uncoordinated bands of the $(EC)_n$–LiX mixtures (Fig. 5b) (Raman band deconvolutions for all of the $(EC)_n$–LiX mixtures are provided in the Supplemental data.). These data, therefore, indicate that the BF_4^- anions, for example, are more extensively coordinated to the Li^+ cations than is found for the PF_6^- anions, as is found for $(AN)_n$–LiX mixtures [2–4].

3.2. $(PC)_n$–LiX Raman analysis

Due to its structural similarity to EC, PC also contains a vibrational band at 712 cm^{-1} which is commonly attributed to a symmetric ring deformation mode [9,14,16,30]. Analysis of the experimental and calculated data indicates that no other bands are significantly perturbed by the addition of a lithium salt in a manner suitable to accurately deconvolute the bands; thus only the 712 cm^{-1} band was analyzed. PC contains a chiral center and

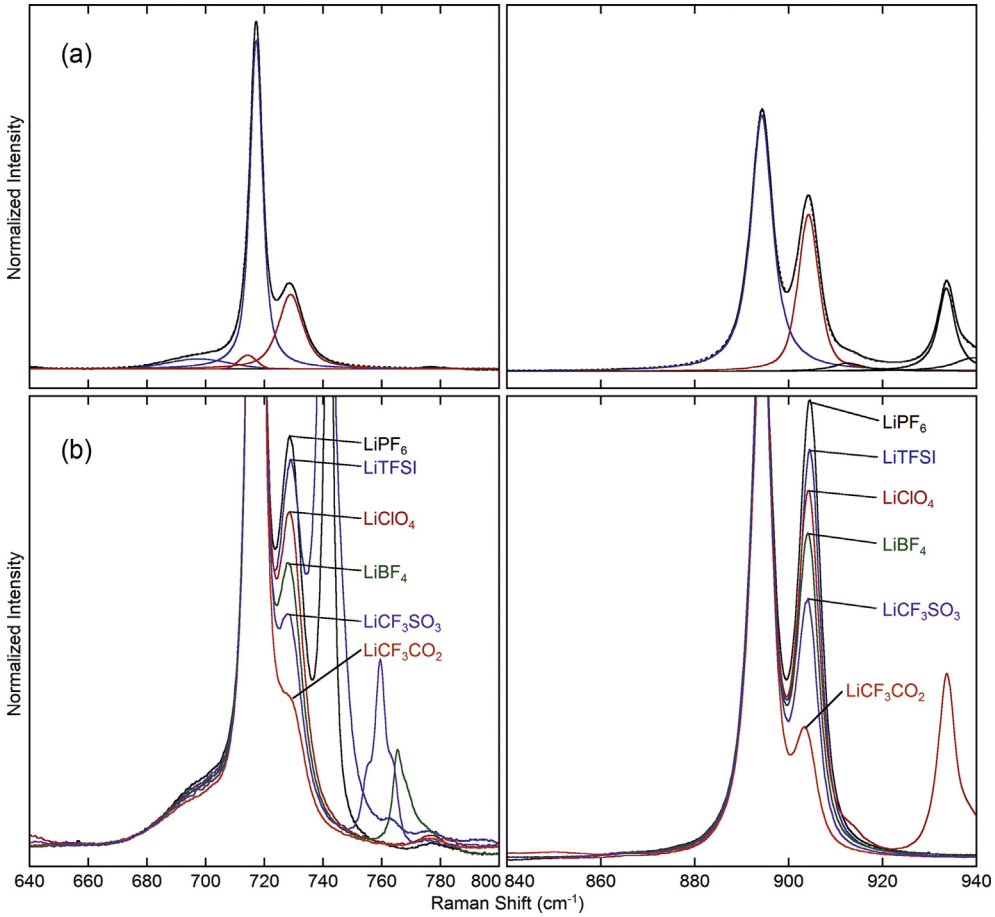

Fig. 5. (a) Deconvoluted experimental Raman spectra of the $(EC)_n$–$LiClO_4$ ($n = 10$) mixture displaying uncoordinated (blue) and Li^+ cation coordinated (red) vibrational bands and (b) Raman band analysis of $(EC)_n$–LiX ($n = 10$ and X = PF_6^-, $TFSI^-$, ClO_4^-, BF_4^-, $CF_3SO_3^-$, $CF_3CO_2^-$) mixtures displaying solvation trends observed due to varying lithium salt (i.e., anion…Li^+ cation) ionic association strengths (note that the additional bands are due to anion vibrational bands) (for interpretation of the references to colour in this figure legend, the reader is referred to the web version of this article).

commercial sources of the solvent are actually racemic mixtures of its isomers. This is demonstrated by a DSC analysis of the isomeric mixtures (Fig. 6) which indicates that such mixtures contain a eutectic point at the equimolar composition with a eutectic melt temperature well below the T_m of each isomer and the same as for commercial (racemic) PC. Preliminary calculations yielded a Raman spectrum that was in disagreement with the experimentally obtained results. These conflicting spectra were originally thought to be attributed to the fact that only the (*S*)-PC conformer was used in the calculations. Experimental analysis of the (*S*)-PC isomer in the liquid phase (−20 to 100 °C), however, yielded a spectrum identical to that for the (*R*)-PC isomer and the racemic PC (Fig. 7). An experimental analysis of the crystalline (*S*)-PC and (*R*)-PC isomers at −80 °C, in contrast, yielded spectra that differ from the crystalline commercial PC (Fig. 7). The variations in these spectra at low temperature indicate that different vibrations are obtained depending upon the conformations of the individual isomers in the solid-state.

Quantum chemical calculations were therefore performed to further investigate the relative conformational energies of PC and their contribution to the overall Raman spectra. Møller–Plesset perturbation theory (MP2), composite G4MP2 and B3LYP functionals were used in conjunction with PCM(PC). Table 4 summarizes the relationship between the O–C–C–O dihedral angle and relative conformational energies for the varying PC conformers. The most accurate geometry is expected from the MP2/Tz calculations. Two low energy conformers were identified, as shown in Fig. 8 for the (*S*)-PC isomer. The cis$^+$ conformer has an O–C–C–O dihedral angle of 24.7°, while the cis$^-$ conformer has an angle of −25.0° for MP2/Tz (Table 4). The B3LYP functional and G4MP2 composite-level calculation, which also uses a DFT-based geometry, predicted smaller magnitudes for the dihedral angle (Table 4). The G4MP2 and MP2/Tz levels are expected to provide the best estimate of the conformational energy difference between the cis$^+$ and cis$^-$ conformers. At 0 K, the cis$^+$ conformer is calculated to be more stable by 0.10–0.23 kcal mol^{-1}, while the cis$^-$ conformer becomes more stable (by 0.06 kcal mol^{-1}) when entropic vibrational contributions are included in the calculations using a temperature of 298 K. Applying the vibrational energy and entropy correction from B3LYP/Tz calculations ($\Delta G - \Delta E$) to the MP2/Tz energy results gives a $\Delta G cis^- - \Delta G cis^+$ value of −0.26 kcal mol^{-1}, indicating that at room temperature one would expect ~40% of the cis$^+$ and ~60% of the cis$^-$ conformers to be present in the liquid.

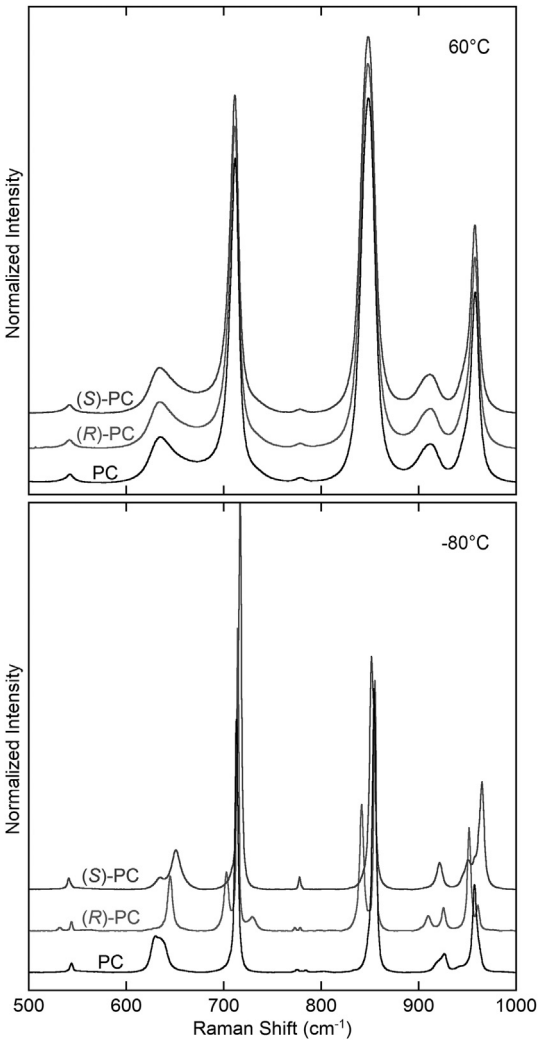

Fig. 7. Comparison of the experimental Raman spectra of the (top, 60 °C) liquid and (bottom, −80 °C) crystalline (*S*)-PC and (*R*)-PC isomers, as well as commercial PC (a racemic mixture of the isomers).

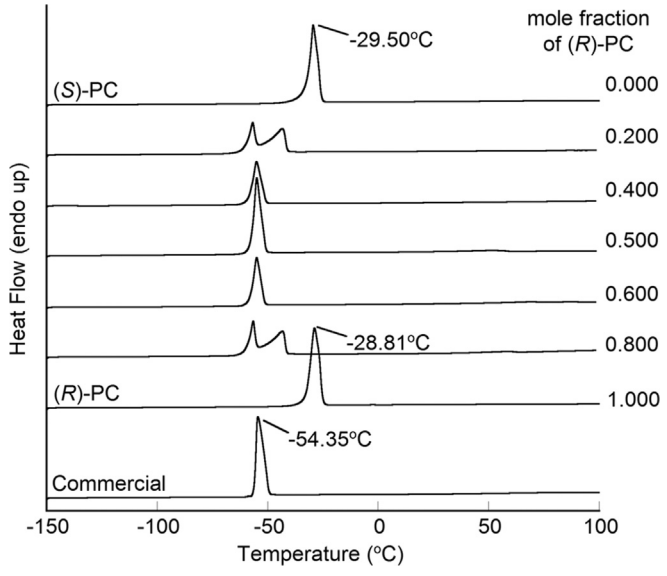

Fig. 6. DSC heating traces (5 °C min^{-1}) of (1−*x*) (*S*)-PC-(*x*) (*R*)-PC isomer mixtures (*x* is mol fraction), as well as commercial PC (a racemic mixture of the isomers).

The calculated Raman spectra were found to be quite different for the cis$^+$ and cis$^-$ conformers in the region of ~600–760 cm^{-1} (Fig. 9). The *ca* 645 cm^{-1} band present for the cis$^+$ conformer completely disappears for the cis$^-$ conformer, while a new band appears at *ca* 740 cm^{-1} for the cis$^-$ conformer. Clearly, the Raman spectra of neither conformer corresponds well to the experimental data, while a combination of the cis$^+$ and cis$^-$ spectra describes the experimentally observed band positions adequately. Specifically, a spectral mixture of 25% cis$^+$ and 75% cis$^-$ fits the relative magnitudes of the experimentally observable bands at ~645 and 712 cm^{-1} quite well. Calculations on a cluster containing one cis$^+$ and three cis$^-$ conformers yielded a Raman spectrum with a ratio of ~0.25 between the 640 and 700 cm^{-1} bands. This ratio is in good agreement with the intensity values obtained experimentally. Additionally, the estimated population of cis$^+$ and cis$^-$ conformers agrees reasonably well with the composition of 40% cis$^+$ and 60% cis$^-$ obtained from the above discussed estimation for $\Delta E cis^+ - cis^-$(MP2/Tz) + ($\Delta G cis^+ - cis^-$(B3LYP/Tz)−$\Delta E cis^+ - cis^-$(B3LYP/Tz)), further supporting the picture that at room temperature the isomeric PC molecules (i.e., (*S*)-PC or (*R*)-PC isomers) consist of a mixture of cis$^+$ and cis$^-$ conformers.

Table 4
PC_1 calculated relative conformational energies (ΔE) and free energies (ΔG) at 298 K for the cis$^+$ and cis$^-$ conformers with the indicated O–C–C–O dihedral angle (φ).

$\varphi_{O-C-C-O}$ (°)	ΔE (kcal mol^{-1})	ΔG (kcal mol^{-1})
B3LYP/Tz		
19.3	0	0
−12.9	0.34	−0.02
B3LYP/6-31 + G(d,p)		
21.0	0	0
−16.0	0.43	0.28
MP2/Tz		
24.7	0	–
−25.0	0.10	–
G4MP2		
17.8	0	0
−13.2	0.23	−0.06

Similar dihedral conformational variability is expected for EC. Various researchers, however, have found that EC tends to adopt the cis$^+$ conformation with a dihedral angle between 24.8° and 29.5° [31–33]. Other experimental results suggest the ring inversion of EC must overcome a barrier of 0.67 kcal mol^{-1} [34]. Based upon the present calculations of the energy requirements for PC to undergo ring inversion, almost all of the conformers with an O–C–C–O dihedral angle between approximately −25° and 25° require less than 0.55 kcal mol^{-1} to undergo conformational transformations (Fig. 10). Due to the low barrier between the cis$^+$ and cis$^-$ conformers (as compared to k_BT which is 0.59 kcal mol^{-1} at room temperature), a fast exchange is expected at room temperature (and above). The EC Raman spectrum is much simpler than that for PC, as there are vibrational contributions principally from a single conformer rather than multiple conformers (the cis$^+$ and cis$^-$ conformers of EC are equivalent). Furthermore, an analysis (B3LYP/Tz level with PCM(PC)) of PC as a function of the O–C–C–O dihedral angle suggests that the frequency of the ~650 cm^{-1} vibration is highly dependent upon the dihedral angle of the conformer. As the dihedral angle changes between the stable conformations (between −25° and 25°), the frequency of the vibrational band changes markedly from *ca* 725 to 630 cm^{-1}, respectively (Fig. 10). Although the PC spectrum is quite complicated due to the existence of its two isomers and the varying conformations for each, an analysis of PC_4 (one cis$^+$, three cis$^-$) does result in reasonably good agreement with experimental data, with the exception of a low intensity band at *ca* 735 cm^{-1} in the calculated spectrum (Fig. S5) which is not evident in the experimental spectrum (Fig. S6). In addition, for the same figures, two calculated bands at *ca* 841 and 856 cm^{-1} are well modeled by a single band in the experimental spectrum.

As noted above, the experimental deconvolution of the spectrum of bulk PC is quite difficult due to the complexity of the Raman signature from the isomers and conformers, and the varying vibrational frequencies of each. Thus, multiple bands are necessary to properly fit the uncoordinated PC bands. Upon Li$^+$ cation

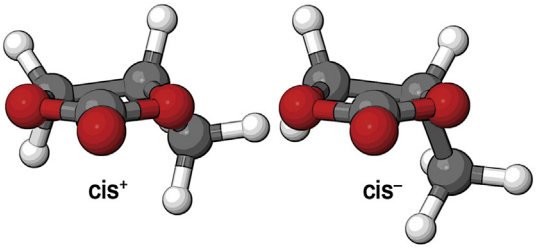

Fig. 8. Low energy cis$^+$ and cis$^-$ conformers of the (*S*)-PC isomer (see Supplemental data for animation).

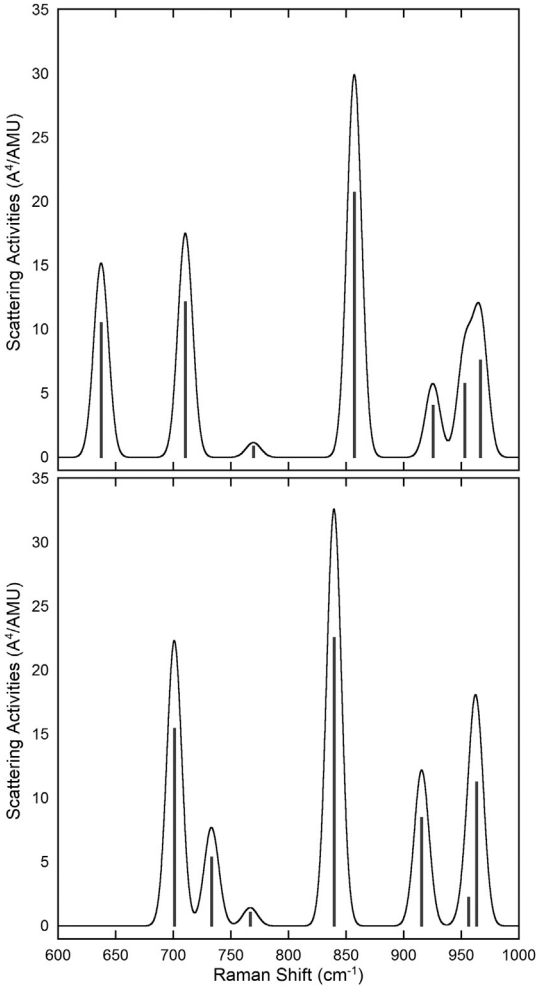

Fig. 9. Raman spectra for the (top) cis$^+$ and (bottom) cis$^-$ conformers of PC from B3LYP/Tz calculations with PCM(PC).

coordination, a new band is observed at ~722 cm^{-1}, but no major perturbation of the 850 cm^{-1} band occurs (Fig. 11). Using the 712 and 722 cm^{-1} bands, solvation numbers were calculated for all of the $(PC)_n$–LiX mixtures. These solvation numbers, although in good agreement with reported literature values [17], were implausibly low. For example, the solvation number calculated for the $(PC)_n$–$LiBF_4$ ($n = 10$) mixture was ~1.35, which is consistent with the literature values of 1.2–1.5 for similar concentrations [17]. In contrast, Yamada et al. report a solvation number of 3.7 for a 1 M PC/$LiClO_4$ mixture [35]. This solvation number, however, was calculated based upon the assumed correction factor of 0.14 for the Raman intensity ratio of the coordinated/uncoordinated PC. The DFT calculations in the present study, however, suggest that the intensity correction factor for the ~722 cm^{-1} band is actually between ~0.87 (cis$^+$ conformer) and ~1.43 (cis$^-$ conformer). Taking the 0.14 correction factor into account, the uncorrected solvation numbers determined by Yamada et al. are even lower than the 1.2–1.5 values reported by Tsunekawa et al. [17] and the ~1.35 calculated in this study. When the dielectric constant (ε) and donor number (DN) of PC (64.95 and 16.4, respectively) are compared to those for EC (90.36 and 15.1, respectively), such a dramatic difference in solvation behavior between the two solvents is unreasonable (the comparable value for EC mixtures is 3.01 in Table 3) [36]. Similarly, the $(EC)_n$–$LiPF_6$ ($n = 20$) data analysis provides a solvation number of 4.15–4.17 (Table 3), as expected since $LiPF_6$ is a highly dissociated salt. The data for a $(PC)_n$–$LiPF_6$ ($n = 20$) mixture,

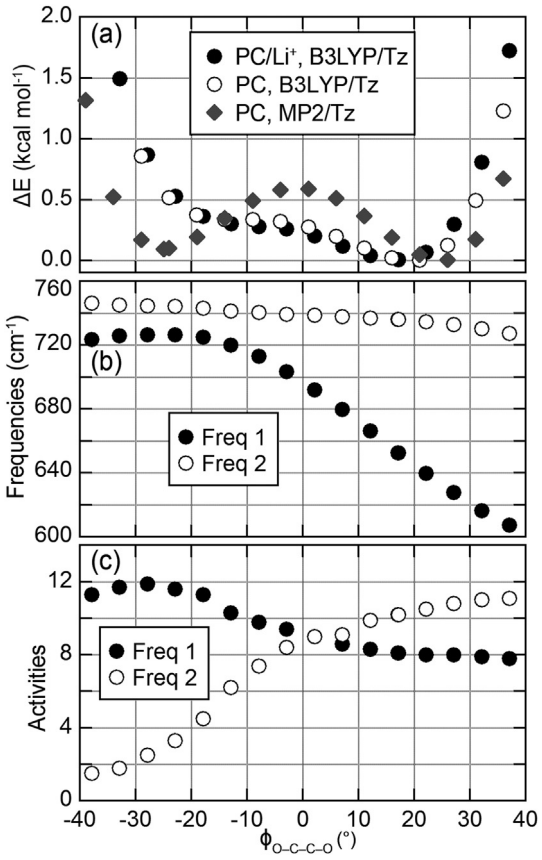

Fig. 10. (a) PC_1 and PC_1/Li^+ conformational energy calculated using MP2/Tz or B3LYP/Tz with PCM(PC) and changes for PC_1/Li^+ of the (b) Raman frequencies and (c) activities as a function of O–C–C–O dihedral angle from B3LYP/Tz calculations with PCM(PC).

in contrast, provide a solvation number of ~1.67. A solvation number this low implies that the Li^+ cations (in order to maintain a 4- or 5-fold coordination) must be highly coordinated by PF_6^- anions. With the dissociated PF_6^- anion, it is unrealistic to expect a high population of CIP and AGG solvates in dilute concentrations (i.e., the $n = 20$ mixture corresponds to ~0.6 mol L^{-1}). Thus, it is highly improbable that the experimentally calculated solvation numbers for the $(PC)_n$–LiX mixtures are representative of the actual solution structure. These numbers also contradicts MD simulation predictions of roughly similar Li^+ coordination in a EC:PC/$LiPF_6$ mixture with a slight preference for PC_n/Li^+ over EC_n/Li^+ coordination in the gas-phase [37].

Quantum chemical calculations can provide additional insight into the problems associated with extracting the Li^+ cation solvation numbers in PC mixtures. Shifts of the PC bands upon Li^+ cation coordination are shown in Table 5. According to these calculations, an observable combined band would be found upon Li^+ cation coordination due to the upshifted $PC(cis^+)_1/Li^+$ band at *ca* 736 cm^{-1} and $PC(cis^-)_1/Li^+$ band at *ca* 741 cm^{-1}, which agrees with the experimentally deconvoluted bands in Fig. 11. But the *ca* 704 cm^{-1} band of the cis^- conformer for uncoordinated PC is also shifted to *ca* 720 cm^{-1} upon Li^+ cation coordination. Therefore, the $PC(cis^-)_1/Li^+$ complex is expected to overlap with the cis^+ band for uncoordinated PC observed at *ca* 715 cm^{-1}. Based upon the calculations for neat PC, the population of the $PC(cis^+)$ conformer is expected to only be 25–40% of the total conformations. Conformational energies for PC_1 and PC_1/Li^+, shown in Fig. 10, indicate that there is no appreciable change in populations as the PC molecules coordinate a Li^+ cation. Due to the minor perturbation of the $PC(cis^+)_1/Li^+$ complex band (723 cm^{-1}), and the expected overlap of the $PC(cis^-)_1/Li^+$ complex band with the uncoordinated $PC(cis^+)$ solvent band, analysis of the $(PC)_n$–LiX mixtures is extremely difficult and inherently full of error. Thus, it is likely not possible to accurately predict the solvation numbers of $(PC)_n$–LiX mixtures from a Raman vibrational analysis of the vibrational band of PC.

4. Conclusions

Understanding the solvation characteristics of electrolyte mixtures is crucial for correlating the electrolyte properties with solvent/ion structures and electrolyte formulations. Although numerous studies have been reported for the determination of the average solvation numbers for Li^+ cations coordinated by cyclic carbonate solvents, these studies have not taken into account the scaling of the Raman intensities for the coordinated solvent bands or the overlap of Raman bands. Thus, considerable inconsistencies have been found for the solvation number values reported in the literature from the evaluation of different EC solvent bands. Using the more rigorous analysis for the reported data in the present study, however, results in solvation numbers that are in exceptional agreement with one another. The solvation trends determined from this analysis of EC are also in excellent agreement with the known ionic association trends of varying anions. In contrast to EC, PC-based electrolytes are difficult to analyze both experimentally and computationally. Commercially available PC is a racemic mixture of (*S*)- and (*R*)-PC isomers. Each of these isomers, however, exists as multiple conformers (cis^+ and cis^-)

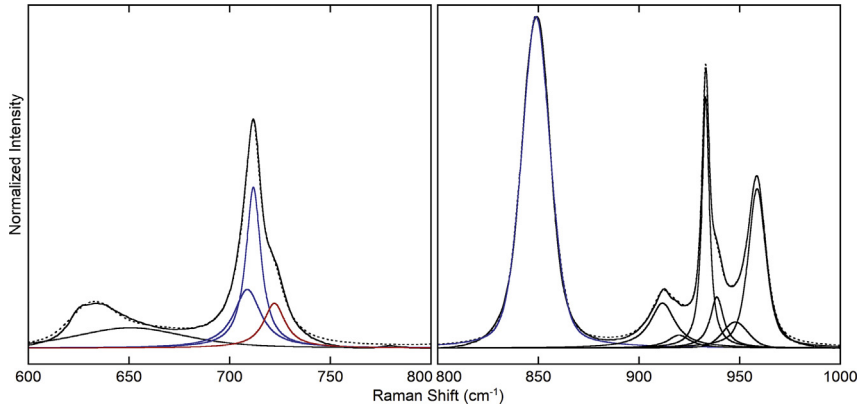

Fig. 11. Deconvoluted experimental Raman spectra of the $(PC)_n$–$LiClO_4$ ($n = 10$) mixture displaying uncoordinated (blue) and Li^+ cation coordinated (red) vibrational bands (for interpretation of the references to colour in this figure legend, the reader is referred to the web version of this article).

Table 5
Shifts of the PC Raman frequencies (cm^{-1}) and activities (S) upon Li^+ cation coordination.

	PC_1	PC_1/Li^+	PC_1	PC_1/Li^+	PC_1	PC_1/Li^+			
	$freq_1$		**$freq_2$**		**$freq_3$**		**$shift_1$**	**$shift_2$**	**$shift_3$**
cis^+	643	653	715	736	856	856	10	21	0
cis^-	704	720	733	741	841	840	16	9	1
	$S(freq_1)$		**$S(freq_2)$**		**$S(freq_3)$**		**$S(PC_1/Li^+)/S(PC_1)$**		
cis^+	9.8	8.1	11.7	10.2	21.7	19.9	0.82	0.87	0.92
cis^-	15.9	10.3	4.3	6.2	24.4	22.1	0.65	1.43	0.90

Calculations using B3LYP/Tz with PCM(PC).

due to an energetically favorable ring inversion and these conformers result in notable differences in the Raman spectral signature. This confluence of spectral features makes the deconvolution of the PC bands daunting and inherently full of error. Nevertheless, a combined quantum chemistry and experimental analysis indicates a slight preference for the PC(cis^-) conformer over the PC(cis^+) conformer at room temperature. Thus, using the bands and scaling factors reported, the average solvation numbers of $(EC)_n$–LiX mixtures can be accurately determined from a Raman spectroscopic analysis, whereas those for $(PC)_n$–LiX mixtures cannot.

Acknowledgments

This work was funded by the U.S. DOE BATT Program (contract number DE-AC02-05-CH11231) for the experimental work related to the pure solvents, the U.S. DOE, Office of Basic Energy Sciences, Division of Materials Sciences and Engineering (contract number DE–SC0002169) for the experimental work related to the solvent-lithium salt electrolytes and the U.S. DOE BATT Program (contract number DE–IA01-11EE003413 through an Interagency Agreement between the U.S. DOE ABR program and the U.S. Army Research Laboratory (ARL)) for the computational work. J.L.A. is grateful for the award of a SMART Graduate Research Fellowship by the SMART Scholarship Program and the American Society for Engineering Education (ASEE).

Appendix A. Supplementary data

Supplementary data related to this article can be found at http://dx.doi.org/10.1016/j.jpowsour.2014.05.107.

References

[1] D.M. Seo, P.D. Boyle, O. Borodin, W.A. Henderson, RSC Adv. 2 (2012) 8014–8019.
[2] D.M. Seo, O. Borodin, S.-D. Han, Q. Ly, P.D. Boyle, W.A. Henderson, J. Electrochem. Soc. 159 (2012) A553–A565.
[3] D.M. Seo, O. Borodin, S.-D. Han, P.D. Boyle, W.A. Henderson, J. Electrochem. Soc. 159 (2012) A1489–A1500.
[4] D.M. Seo, O. Borodin, D. Balogh, M. O'Connell, Q. Ly, S.-D. Han, S. Passerini, W.A. Henderson, J. Electrochem. Soc. 160 (2013) A1061–A1070.
[5] S.-D. Han, O. Borodin, J.L. Allen, D.M. Seo, D.W. McOwen, S.-H. Yun, W.A. Henderson, J. Electrochem. Soc. 160 (2013) A2100–A2110.
[6] S.-A. Hyodo, K. Okabayashi, Electrochim. Acta 34 (1989) 1551–1556.
[7] S.-A. Hyodo, K. Okabayashi, Electrochim. Acta 34 (1989) 1557–1561.
[8] E. Cazzanelli, P. Mustarelli, F. Benevelli, G.B. Appetecchi, F. Croce, Solid State Ionics 86–88 (1996) 379–384.
[9] E. Cazzanelli, F. Croce, G.B. Appetecchi, F. Benevelli, P. Mustarelli, J. Chem. Phys. 107 (1997) 5740–5747.
[10] M. Morita, Y. Asai, N. Yoshimoto, M. Ishikawa, J. Chem. Soc. Faraday Trans. 94 (1998) 3451–3456.
[11] Z. Wang, B. Huang, R. Xue, L. Chen, X. Huang, J. Electrochem. Soc. 145 (1998) 3346–3350.
[12] B. Klassen, R. Aroca, M. Nazri, G.A. Nazri, J. Phys. Chem. B 102 (1998) 4795–4801.
[13] M. Castriota, E. Cazzanelli, I. Nicotera, L. Coppola, C. Oliviero, G.A. Ranieri, J. Chem. Phys. 118 (2003) 5537–5541.
[14] D. Battisti, G.A. Nazri, B. Klassen, R. Aroca, J. Phys. Chem. 97 (1993) 5826–5830.
[15] K. Kondo, M. Sano, A. Hiwara, T. Omi, M. Fujita, A. Kuwae, M. Iida, K. Mogi, H. Yokoyama, J. Phys. Chem. B 104 (2000) 5040–5044.
[16] X. Xuan, J. Wang, J. Tang, G. Qu, J. Lu, Spectrochim. Acta 56A (2000) 2131–2139.
[17] H. Tsunekawa, A. Narumi, M. Sano, A. Hiwara, M. Fujita, H. Yokoyama, J. Phys. Chem. B 107 (2003) 10962–10966.
[18] E.E. Zvereva, A.R. Shagidullin, S.A. Katsyuba, J. Phys. Chem. A 115 (2011) 63–69.
[19] S.I. Gorelsky, SWizard Program, Revision 4.7, http://www.sg-chem.net./.
[20] S.I. Gorelsky, A.B.P. Lever, J. Organomet. Chem. 635 (2001) 187–196.
[21] B. Fortunato, P. Mirone, G. Fini, Spectrochim. Acta 27A (1971) 1917–1927.
[22] J.R. Durig, G.L. Coulter, D.W. Wertz, J. Mol. Spectrosc. 27 (1968) 285–295.
[23] K.L. Dorris, J.E. Boggs, A. Danti, L.L. Altpeter, J. Chem. Phys. 46 (1967) 1191–1193.
[24] G. Fini, P. Mirone, B. Fortunato, J. Chem. Soc. Faraday Trans. 2 69 (1973) 1243–1248.
[25] H.N. Al-Jallo, F.N. Al-Azawi, Spectrochim. Acta 34A (1978) 819–823.
[26] M. Masia, M. Probst, R. Rey, J. Phys. Chem. B 108 (2004) 2016–2027.
[27] M. Masia, R. Rey, J. Phys. Chem. B 108 (2004) 17992–18002.
[28] O. Borodin, G.D. Smith, J. Phys. Chem. B 113 (2009) 1763–1776.
[29] W.A. Henderson, J. Phys. Chem. B 110 (2006) 13177–13183.
[30] G.J. Janz, J. Ambrose, J.W. Coutts, J.R. Downey Jr., Spectrochim. Acta 35A (1979) 175–179.
[31] J.-C. Soetens, C. Millot, B. Maigret, I. Bakó, J. Mol. Liq. 92 (2001) 201–216.
[32] P.M. Matias, G.A. Jeffrey, L.M. Wingert, J.R. Ruble, J. Mol. Struct. 184 (1989) 247–260.
[33] C.J. Brown, Acta Crystallogr. 7 (1954) 92–96.
[34] J.L. Alonso, R. Cervellati, A.D. Esposti, D.G. Lister, P. Palmieri, J. Chem. Soc. Faraday Trans. 2 82 (1986) 337–356.
[35] Y. Yamada, Y. Koyama, T. Abe, Z. Ogumi, J. Phys. Chem. C 113 (2009) 8948–8953.
[36] J.M.G. Barthel, H. Krienke, W. Kunz, in: H. Baumgartel, E.U. Franck, W. Grunbein (Eds.), Physical Chemistry of Electrolyte Solutions: Modern Aspects, Springer, Wurzburg, Germany, 1998.
[37] A.W. Cresce, O. Borodin, K. Xu, J. Phys. Chem. C 116 (2012) 26111–26117.